Ferromagnetism in Hydrogenated Graphene Nanopore Arrays

K. Tada,[1] J. Haruyama,[1,*] H. X. Yang,[2] M. Chshiev,[2] T. Matsui,[3] and H. Fukuyama[3]

[1]*Faculty of Science and Engineering, Aoyama Gakuin University, 5-10-1 Fuchinobe, Sagamihara, Kanagawa 252-5258, Japan*
[2]*SPINTEC, CEA/CNRS/UJF-Grenoble 1/Grenoble-INP,38054, Grenoble cedex 9, France*
[3]*Department of Physics, University of Tokyo, 7-3-1 Hongo, Bunkyo-ku, Tokyo 113-8656, Japan*

(Received 4 August 2011; published 15 November 2011)

Theoretically, the so-called zigzag edge of graphenes provides localized electrons due to the presence of flat energy bands near the Fermi level. Spin interaction makes the localized spins strongly polarized, yielding ferromagnetism. However, in most experimental studies, ferromagnetism has been observed in uncontrollable and complicated carbon-based systems. Here, we fabricate graphenes with honeycomblike arrays of hexagonal nanopores, which have a large ensemble of hydrogen-terminated and low-defect pore edges that are prepared by a nonlithographic method (nanoporous alumina templates). We observe large-magnitude ferromagnetism derived from electron spins localizing at the zigzag nanopore edges. This promises to be a realization of graphene magnets and novel spintronic devices.

DOI: 10.1103/PhysRevLett.107.217203 PACS numbers: 75.70.−i, 75.30.−m, 75.50.Dd, 75.75.−c

Ferromagnetism in carbon-based materials is unique, because only *s* and *p* orbital electrons cause it. In particular, edge atomic structures of graphene have been of great interest [1–25].

The localized electron spins at the zigzag edge of graphene (Fig. 5) with flat bands near the Fermi level (E_F) [1,8] are stabilized and strongly polarized depending on the exchange interaction between the two edges, which forms a maximum spin ordering in these orbitals similar to the case of Hund's rule for atoms (e.g., as in a graphene nanoribbon (GNR) that is a 1D restriction of graphene with edges on both longitudinal sides [Figs. 5(b) and 5(c)] [1–7,15–17], in a graphene with (hexagonal) nanopore arrays [Figs. 1(b) and 5(a)] [11,18,19,22], and in graphene nanoflakes [12]). This determines the appearance of (anti) ferromagnetism in GNRs [3,5–7,11,12]. Moreover, spin ordering strongly depends on the termination of edge carbon atoms (dangling bonds) by foreign atoms [e.g., hydrogen (H)] and those numbers, which result in the formation of edge π and σ orbitals [3,24].

From another theoretical viewpoint, Lieb's theorem predicts that an increase in the difference between the number of removed *A* and *B* sites of the graphene bipartite lattice at zigzag edges induces net magnetic moments and yields ferromagnetism, particularly in nanosize graphene flakes [12] and nanopores [14,22].

However, damages, defects, and disorder introduced during the lithographic fabrication process of edges have prevented observation of ferromagnetism to arise from zigzag-edge-localized spins in graphenes. In the present study, low-defect graphene nanopore arrays (GNPAs) with honeycomblike arrays of hexagonal nanopores [Fig. 1(b)] were fabricated on a large ensemble of mechanically exfoliated graphenes by using a nanoporous alumina template [NPAT: Fig. 1(a)] as an etching mask, followed by low-power Ar-gas etching and high-temperature (800 °C) annealing in high vacuum and H_2 atmosphere [Supplemental Material (SM) (1)–(5) [26]]. This method at least gives three significant advantages [SM (1) [26]].

Figure 1(a) shows the top view of a scanning electron microscopy (SEM) image of NPAT (Al_2O_3) [25] that was used as the etching mask to form the nanopore array on graphene [SM (1) [26]]. Atomic force microscopy (AFM) images of a GNPA formed by carefully optimized low-power Ar-gas etching using NPAT masks are presented in Fig. 1(b). It provides clear evidence of the hexagonal shape of the nanopores [SM (2)–(4) [26]]. Figure 1(c) shows a scanning tunnel microscope (STM) image obtained in an approximately 10-layer GNPA with H termination [SM (5) [26]]. The figure demonstrates the presence of high electronic density of states (EDOS) (white regions) at the pore edges on the surface of a graphene layer [21] and consequent electron localization, although the high EDOS is smeared because of the blurring by the tip of the STM probe top. This suggests the possible presence of a zigzag atomic structure at the nanopore edges [Fig. 5(a)].

Figures 1(d) and 1(e) show typical Raman spectra of a GNPA prior to and after annealing, respectively. They emphasize that the intensity of *D* peak, $I(D)$, is significantly reduced after annealing and, thus, the $I(D)/I(G)$ value drastically decreases from 0.6–0.8 to less than ~0.5 by annealing [inset of Fig. 1(e)]. In particular, samples 1–4 exhibit $I(D)/I(G)$ as low as below 0.2. The low $I(D)/I(G)$ values conventionally suggest high-quality carbon crystals with a low volume of defects (disorder, impurities). This result is very different from those reported in previous studies of ferromagnetism in carbon-based systems, where a large volume of defects or disorder was present [27]. In Ref. [15], we actually proved that defects and disorders in GNRs could be drastically reduced by high-temperature annealing at 800 °C.

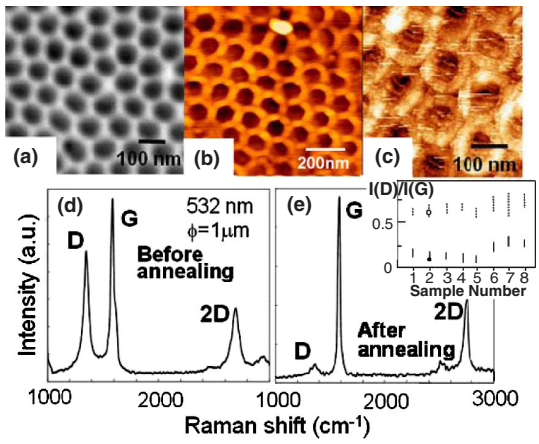

FIG. 1 (color online). (a) SEM image of nanoporous alumina template (NPAT) with mean pore diameter $\phi \sim 80$ nm and mean interpore spacing $W \sim 20$ nm (i.e., W corresponds to the GNR width; see Fig. 5(a) [SM (1) [26]]). (b) AFM image of a GNPA formed by using (a) as an etching mask, which proves hexagonal shape of nanopores. (c) STM image of the approximately 10-layer GNPA obtained at 80 K in a constant-current mode. Lighter regions at pore edges denote higher EDOS. (d),(e) Typical Raman spectra of a GNPA (d) prior and (e) after annealing at 800 °C, taken with a laser excitation of 532 nm and 0.14 mW incident power at room temperature. Because the laser beam diameter ϕ used for the measurement is 1 μm, the result reflects edge information of ~60 pores. Inset of (e): distribution of $I(D)/I(G)$ in eight samples. Fifteen points at five different positions were observed per sample. Dotted and solid lines above and below 0.5 denote $I(D)/I(G)$ prior and after annealing, respectively. Black and open symbols correspond to main panels of (d) and (e), respectively.

More importantly, the low $I(D)/I(G)$ value implies not only a reduction of defects but also an enhanced alignment of pore boundaries to the pure zigzag edges by reconstruction due to high-temperature annealing from the following two reasons, although we have not performed intentional alignment of the pore edges to pure zigzag structure. (1) Ref. [23] reported that edge chirality can be distinguished by observation of $I(D)$ of graphene edges being stronger (weaker) at the armchair (zigzag) edges. This is because the double resonance process, which induces D peak, can be fulfilled only at an armchair edge when the one-dimensional character of the edge is considered [23]. Indeed, Ref. [23] exhibited $I(D)/I(G)$ value <0.1 for observation of zigzag edge of graphene flakes by using angle-dependent Raman spectroscopy with polarized laser beam. It is qualitatively consistent with Fig. 1(e). (2) The low $I(D)/I(G)$ values are also qualitatively consistent with the values reported for GNPAs in Ref. [18], whose hexagonal-pore boundaries are intentionally aligned along the carbon hexagonal lattice by a specified method, resulting in formation of the pure zigzag pore edges. This is also consistent with the STM observation [Fig. 1(c)].

We did not intentionally align pore-edge atomic structures to zigzag unlike Ref. [18]. References [13,14], however, suggested that the zigzag edge is the most stable chemically and that armchair-based edges are reconstructed to zigzag after electron beam (EB) irradiation for pore edges and STM Joule heating for long edges of overlapped graphenes [SM (9),(10) [26]]. This stability may be simply understood by difference in the number of carbon atoms bonded to two neighboring carbon atoms (dangling bonds) for the zigzag edge (i.e., one such atom) and arm chair edges (two such atoms) [14]. After the removal of such atoms, the armchair edge requires energy 2 times larger than zigzag in order to repair the removed atoms and, thus, becomes unstable. In our system, the etching process for formation of the nanopores and narrow (~20 nm) GNRs might give the effect similar to EB irradiation and Joule heating.

Figure 2(a) shows a magnetization curve for the H-terminated monolayer of GNPA [sample 2 in the inset of Fig. 1(e)] at 2 K [SM (5) [26]]. A ferromagnetic-hysteresis loop with large amplitude is clearly observed. In contrast, this feature becomes a diamagnetismlike weak hysteresis loop for oxygen-terminated GNPAs [Fig. 2(b)] [SM (7) [26]]. Bulk graphenes without nanopores and those assembled with NPATs show mostly no such features even after H_2 annealing [Figs. 2(c) and 2(f)] [SM (8) [26]], implying that no parasitic factors (e.g., defects, impurities) of bulk graphenes contribute to the ferromagnetism. It is also confirmed that the features observed at 2 K appear even at room temperature with a larger magnitude of the hysteresis loops [Figs. 2(d)–2(f)], although the amplitude of magnetization decreases.

In addition to sample 2, samples 1, 3, and 4 show the low $I(D)/I(G)$ values [the inset of Fig. 1(e)] exhibited similar ferromagnetism. Moreover, no damages or impurities are reconfirmed in most of bulk-graphene regions, because mechanically exfoliated bulk graphenes show an extremely low $I(D)/I(G)$ ratio ($\ll 0.1$) and a high 2D peak intensity in the Raman spectroscopy. This is consistent with the absent ferromagnetism in Figs. 2(c) and 2(d) as mentioned above. These results strongly suggest that the observed ferromagnetism [Figs. 2(a) and 2(d)] is associated with the H-terminated zigzag nanopore edges.

To reconfirm the contribution of zigzag pore edges to the observed ferromagnetism, the correlation between the interpore spacing [corresponding to the width of the GNR, W; Fig. 5(a)] and the magnetization was measured as shown in Fig. 3. We find that the magnitude of the residual magnetization is inversely proportional to the W value [the inset of Fig. 3(b)]. This result is qualitatively consistent with theories for GNR model according to which the edge spin stability and ordering of a zigzag-edge GNR are determined by the exchange interaction between the two edges leading to vanishing of ferromagnetic edge spin ordering with increase of W [2,5]. Such behavior cannot be attributed to the ferromagnetism originating from the defects located only at nanopore edges or in the bulk

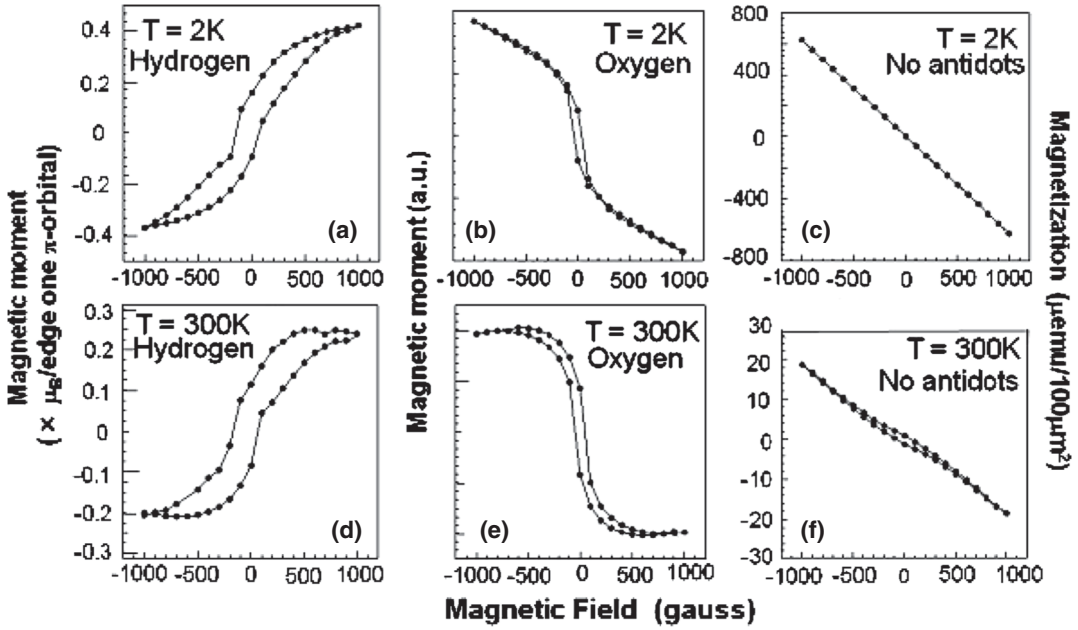

FIG. 2. Magnetization of monolayer GNPAs [SM (5) [26]] with $\phi \sim 80$ nm and $W \sim 20$ nm for (a),(d) hydrogen-terminated edges; (b),(e) oxygen-terminated nanopore edges; and (c),(f) bulk graphene without nanopore arrays. dc magnetization was measured by a superconducting quantum interference device (SQUID; Quantum Design) at 2 K and at room temperature for panels (a)–(c) and panels (d)–(f), respectively. Magnetic fields were applied perpendicular to GNPAs. The vertical axes in panels (a) and (d) denote magnetic moment per localized-edge π orbital, assuming monohydrogenation of individual edge carbon atoms [Fig. 5(c)]. For (d), difference in magnetic moment between upper and lower curves of hysteresis loop at $H = 0$ (residual magnetization $B_r \times 2$) is $\sim 0.2\ \mu_B$ and the loop width at zero magnetic moment (coercivity $H_c \times 2$) is ~ 260 G.

graphene between nanopores. Indeed, in the former case ferromagnetism would be mostly independent of W, while in the latter case ferromagnetism amplitude would increase with an increase of W. Consequently, we conclude that the observed ferromagnetism is not of parasitic origins (e.g., defects, impurities) but should be purely attributed to H-terminated nanopore edges.

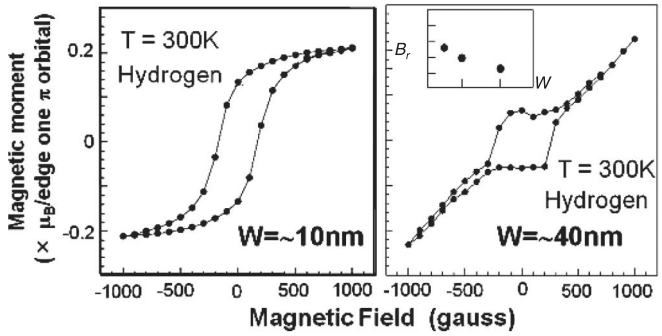

FIG. 3. Correlation of the magnetization with the mean interpore spacing W of GNPA. W corresponds to the mean width of GNRs. Mean pore diameter ($\phi \sim 80$ nm) was kept through all samples. Values of (residual magnetization $B_r \times 2$) and (coercivity $H_c \times 2$) for (a) and (b) are $\sim 0.28\ \mu_B$ and ~ 400 G, and $\sim 0.12\ \mu_B$ and ~ 500 G, respectively. Inset of (b). Residual magnetization at 300 K as a function of W, determined from Fig. 2(d) and this figure.

For further reconfirmation of correlation of the observed ferromagnetism with the zigzag pore edge, we performed magnetic force microscope (MFM) observations (Fig. 4). The interpore regions, which correspond to GNRs, exhibit mostly uniform darker color that means higher density of polarized spins, in all parts. This suggests that the observed ferromagnetism is attributed not to defects (disorder), which exists at random, but to all interpore GNR regions, although poor resolution does not allow direct observation of edge-localized spins. In particular, the parts indicated by

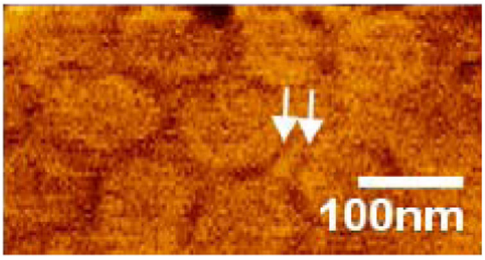

FIG. 4 (color online). Magnetic force microscope (MFM) images of an H-terminated GNPA on SiC substrate, which showed ferromagnetism similar to Fig. 2. CoPtCr-coated Si probe was used for the measurements with a tapping mode, in which the distance between the MFM tip and sample surface was kept in a constant value [SM (12) [26]]. Darker colors mean higher density of polarized spins. In particular, the parts indicated by two arrows evidently imply pore-edge lines.

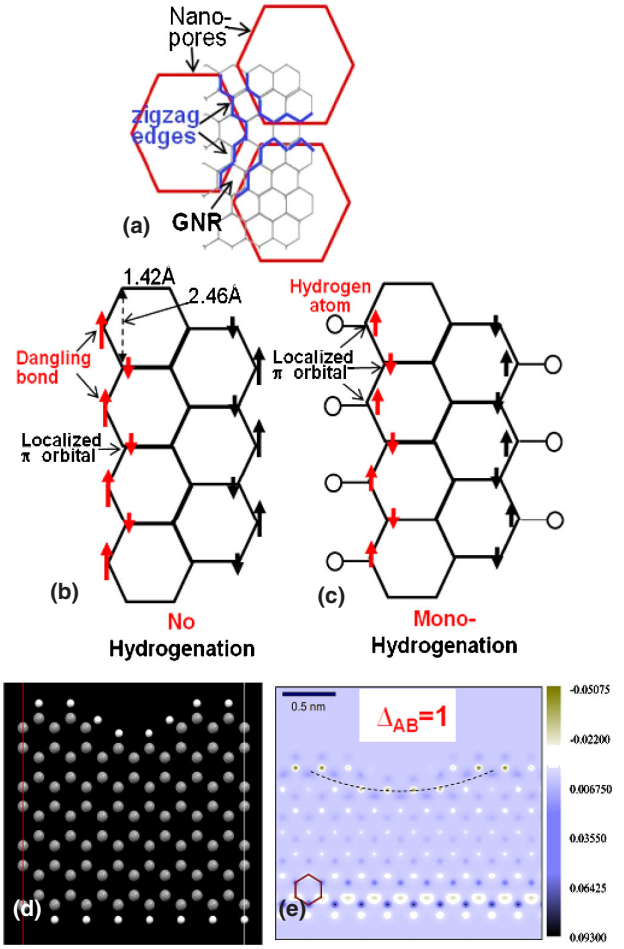

FIG. 5 (color online). (a) Schematic view of honeycomblike hexagonal nanopores formed on graphene, which shows the case that the pore boundaries are aligned with the carbon hexagonal lattice of graphene to form a zigzag edge. Narrow spaces between two pores correspond to GNRs. The actual structure has a larger number of hexagonal carbon unit cells per GNR (~ 40 nm length and ~ 20 nm width). This GNPA structure brings at least three large advantages [SM (1) [26]]. (b),(c) Spin configuration of pure zigzag-edge GNR models (b) without and (c) with mono-H termination. The spin interaction between two zigzag edges yields and stabilizes the ferromagnetic edge spin ordering by maximizing exchange energy gain. Arrows denote localized edge spin moments. In (c), open symbols denote a single hydrogen atom. Actual structure has a larger number of columns of carbon hexagonal unit cells. For (b), only the dangling bond states contribute to the total magnetic moment with a large exchange splitting. Although this ground state gives antiferromagnetic spin alignment with zero total-magnetism, ferromagnetic configuration is shown here just for explanation of the calculation method for magnetism. For (c), edge dangling bonds are monohydrogenated, resulting in localized-edge π-orbital states. (d) Structure of hydrogen passivated quasi-GNR, which assumes slight curvature, used for first-principles calculations based on Lieb's theorem. The dark and white atoms are carbon and hydrogen, respectively. (e) Calculated spin-density distribution of quasi-GNR with $\Delta_{AB} = 1$ (the difference between the number of removed A and B sites of the graphene sublattices at zigzag edges) for (d). It gives the edge magnetic moment of 0.25 μ_B.

two arrows evidently imply contribution of the pore edges to ferromagnetism.

The present nonlithographic method with careful Ar-gas etching realizes the pore-edge derived ferromagnetism by minimizing damage to the nanopore edges [SM (3) [26]]. The present GNPAs have also strong advantage [SM (1) [26]] compared with previous other carbon-related systems, because they have a simple, highly reproducible, and controllable structure (i.e., consisting only of a silicon substrate and GNPAs). To date, approximately 50% of the samples [5 of the 11 samples measured, which include samples 1–4 showing the low $I(D)/I(G)$ values in the inset of Fig. 1(e)] have shown ferromagnetism [SM (5),(9) [26]].

In order to estimate the magnetic moment of edge carbon atoms which contribute to ferromagnetism (Fig. 2), we employ the GNR model assuming zigzag pore edges at all regions. Assuming that only edge dangling bonds have localized spin moments, the magnetic moment per edge dangling bond prior to H termination [Fig. 5(b)] is calculated according to SM (14) [26]. Then, the magnetic moment per edge dangling bond is estimated to be $(1.2 \times 10^{-23})/(\mu_B = 9.3 \times 10^{-24}) \sim 1.3\ \mu_B$, where μ_B is the Bohr magneton.

Next, after H annealing at high temperature, edge dangling bonds of a GNR are terminated by H atoms [3,5–7,28] [SM (6),(11) [26]]. Basically, three terminations should be considered: (1) mono-H termination for both edges, (2) di-H termination for both edges, and (3) mono-H termination for one edge and di-H termination for the other edge. From a theoretical viewpoint, case (1) results in the formation of sp^2 and π orbitals [Fig. 5(c)], which yields a flat energy band at $2\pi/3 \leq k \leq \pi$ in the Brillouin zone with electron localization. In contrast, case (2) results in the formation of sp^3 and σ orbitals because of the tetrahedral coordination of 2 H atoms. It forms a flat band at $0 \leq k \leq 2\pi/3$ with suppressed electron localization. Case (3) produces a flat band at $0 \leq k \leq \pi$ with entirely localized electrons.

The type of edge H-termination could not be confirmed in the present experiment. However, we argue that our case corresponds to case (1) from the following reason. The mono-H termination of the edge dangling bond decreases its magnetic moment to one μ_B. The magnetic moment of one localized-edge π orbital is, therefore, estimated to be as large as $(\sim 1.3\ \mu_B – 1\ \mu_B) = \sim 0.3\ \mu_B$. This is in fairly good agreement with the theoretical contribution of the π-orbital state to the edge magnetic moment of $\sim 0.3\ \mu_B$ in a zigzag-edged GNR within the ferromagnetically ordered spin configuration [5]. The observed ferromagnetism is stable at least for one week even under air atmosphere at room temperature. Why mono-H termination for both edges of a GNR (i.e., edges of the hexagonal pores) is such stable should be clarified in future [SM (11) [26]].

We have estimated the edge magnetization based on a GNR model with zigzag edges, assuming the presence of

pure zigzag pore edges at all parts of our GNPAs. One can admit, however, that a small disorder may still be present in actual pore edges, because the $I(D)/I(G)$ values in Fig. 1(e) are still not extremely low. In order to elucidate the influence of such residual small-volume disorder on magnetism of GNPA, we performed systematic first-principles calculations of electronic and magnetic properties of quasi-GNR structures [Fig. 5(d)] based on Lieb's theorem [22], which assumes the slightly curved upper edge (i.e., disorder). Interestingly, the ground state of quasi-GNR structure turned out to be ferromagnetic. The calculated net magnetic moment follows Lieb's theorem with local moments up to 0.25 μ_B per edge atom and they depend on magnitude of the assumed edge curvature. These values agree fairly well with the value estimated from the GNR model. As an example, in Fig. 5(e) we present the calculated spin-density distribution for the quasi-GNR structure shown in Fig. 5(d). In order to determine which models [Figs. 5(c) and 5(d)] are more relevant to the actual structures, observation of pore-edge atomic structures is indispensable [SM (9) [26]]. Our observations pave the way towards the realization of room temperature ferromagnetism in graphene and novel spintronic devices [SM (13) [26]].

K. T. and J. H. thank K. Fujita, Y. Hashimoto, E. Endo, S. Katsumoto, Y. Iye, M. Yamamoto, S. Tarucha, K. Wakabayashi, M. Koshino, T. Ando, T. Enoki, T. Muranaka, J. Akimitsu, T. Yamaoka, N. Nagaosa, H. Aoki, S. Roche, P. Kim, X. Jia, and M. S. Dresselhaus for their technical contribution, fruitful discussions, and encouragement. This work at Aoyama Gakuin was partly supported by a grant-in-aid for scientific research and a High-Technology Research Center Project for private universities in MEXT. M. C. and H. X. Y. acknowledge support by French ANR PNANO project ''Nanosim-Graphene'' and Grenoble Nanosciences Foundation.

*To whom correspondence should be addressed.
J-haru@ee.aoyama.ac.jp

[1] K. Nakada *et al.*, Phys. Rev. B **54**, 17 954 (1996).
[2] M. Fujita *et al.*, J. Phys. Soc. Jpn. **65**, 1920 (1996).
[3] K. Kusakabe and M. Maruyama, Phys. Rev. B **67**, 092406 (2003).
[4] S. Okada and A. Oshiyama, Phys. Rev. Lett. **87**, 146803 (2001).
[5] H. Lee *et al.*, Phys. Rev. B **72**, 174431 (2005).
[6] R. G. A. Veiga *et al.*, J. Chem. Phys. **128**, 201101 (2008).
[7] H. Lee *et al.*, Chem. Phys. Lett. **398**, 207 (2004).
[8] Y. Niimi *et al.*, Phys. Rev. B **73**, 085421 (2006).
[9] Y-W. Son *et al.*, Phys. Rev. Lett. **97**, 216803 (2006).
[10] L. Yang *et al.*, Phys. Rev. Lett. **99**, 186801 (2007).
[11] N. Shima *et al.*, Phys. Rev. Lett. **71**, 4389 (1993).
[12] J. F. Rosser and J. J. Palacios, Phys. Rev. Lett. **99**, 177204 (2007).
[13] X. Jia *et al.*, Science **323**, 1701 (2009).
[14] C. O. Girit *et al.*, Science **323**, 1705 (2009).
[15] T. Shimizu *et al.*, Nature Nanotech. **6**, 45 (2010).
[16] M. Y. Han *et al.*, Phys. Rev. Lett. **104**, 056801 (2010).
[17] X. Wang *et al.*, Phys. Rev. Lett. **100**, 206803 (2008).
[18] B. Krauss *et al.*, Nano Lett. **10**, 4544 (2010).
[19] J. Bai *et al.*, Nature Nanotech. **5**, 190 (2010).
[20] Y-W. Son *et al.*, Nature (London) **444**, 347 (2006).
[21] M. Otani *et al.*, Phys. Rev. B **81**, 161403(R) (2010).
[22] H. Yang *et al.*, arXiv:1103.4188.
[23] Y. You *et al.*, Appl. Phys. Lett. **93**, 163112 (2008).
[24] D. Soriano *et al.*, Phys. Rev. Lett. **107**, 016602 (2011).
[25] I. Takesue *et al.*, Phys. Rev. Lett. **96**, 057001 (2006).
[26] See Supplemental Material at http://link.aps.org/supplemental/10.1103/PhysRevLett.107.217203 for sample fabrication methods, calculation methods for edge magnetization, and so on.
[27] J. Cervenka *et al.*, Nature Phys. **5**, 840 (2009).
[28] T. Enoki *et al.*, Solid State Commun. **149**, 1144 (2009).